Research Article

Parity Violation and Magnetic Helicity on Cosmological Scales: From Turbulent Baryogenesis to Galaxy Clusters

Alexander Bershadskii[1]

1. ICAR, Israel

Using results of numerical simulations and the CMB data obtained by the Planck satellite mission and Atacama cosmology telescope, it is shown that chaotic/turbulent parity violation localized in long-lived magnetic blobs dominated by magnetic helicity takes place at cosmological lepto/baryogenesis. Analogous phenomenon has also been confirmed for magnetic fields in galaxy clusters. Despite the vast differences in the values of physical parameters and spatio-temporal scales between the numerical simulations and the cosmic observations, there is a quantitative agreement between the results of the cosmic observations and the numerical simulations in the frames of the distributed chaos notion.

Corresponding author: A. Bershadskii, bershads@gmail.com

I. Introduction

Baryogenesis at an earlier stage of universe development is one of the main candidates for magnetogenesis. The parity (reflection symmetry) violation and a nonzero magnetic helicity appearance are a crucial part of these processes (see, for instance, a review[1] and references therein). The magnetic helicity can also be a key for solving the baryon asymmetry problem[2]. The lepto/baryogenesis epoch was rather turbulent because about all created baryons and antibaryons (as well as electrons and positrons) were annihilated producing a huge amount of energy.

The point-wise helicity production is an inherent property of the 3D chaotic/turbulent motion of the plasmas/fluids. In such flows the helicity appears spontaneously (even in the cases of zero net helicity) in pairs of patches having opposite signs of the helicity so that the net helicity remains zero. This

phenomenon takes place in both non-magnetic (kinetic helicity) and magnetic (magnetic helicity) cases[3][4][5][6]. In the latter case, a part of the patches is transformed into long-lived magnetic blobs with sign-defined helicity and reduced dissipation[6][7]. Despite the net helicity is remaining zero the absolute value of the total sum of the sign-defined helicities of the magnetic blobs $|I^{\pm}|$ ($I^{+} = -I^{-}$) can be used as a measure of spontaneous parity violation (see Section 4 for more detail). In the present paper, we will study how this measure of parity violation is related to a measure of randomness of the chaotic/turbulent magnetic field (some other types of cosmological parity violation built on intrinsic reflection asymmetry of the particles one can find in a recent review[8] and references therein).

The conception of smoothness can be used to quantify the levels of randomness of the chaotic/turbulent dynamical regimes. Indeed, the stretched exponential spectrum

$$E(k) \propto \exp -(k/k_{\beta})^{\beta} \tag{1}$$

is a characteristic feature of smooth chaotic dynamics. Here $1 \geq \beta > 0$ and k is the wavenumber.

The value of the $\beta = 1$ characterizes the deterministic chaos (see, for instance,[9][10][11][12][7] and references therein):

$$E(k) \propto \exp{(-k/k_{c})}. \tag{2}$$

When $1 > \beta$ the smooth chaotic dynamics can be already non-deterministic, this type of smooth dynamics can be called ‘distributed chaos’ (the term will be clarified below). Another term “soft turbulence” (suggested by[13]) can be also appropriate.

The parameter β could be used as an informative measure of randomization. Namely, the further the value of β is from the $\beta = 1$ (which corresponds to the deterministic chaos) the more significant the system’s randomization. The smaller parameter β values are considered a precursor of hard turbulence. The scaling power spectrum is a characteristic feature of non-smooth random dynamics (the hard turbulence in terms of[13]).

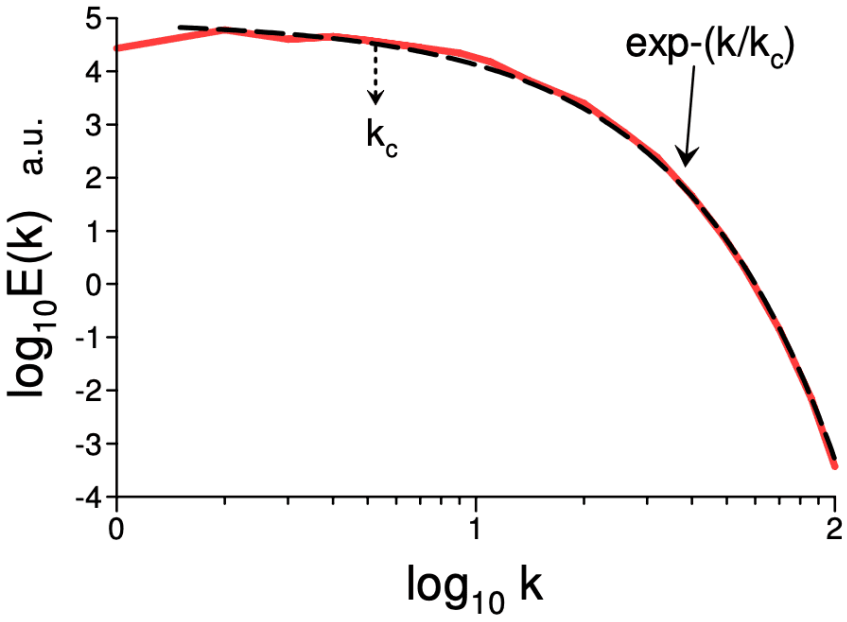

Figure 1. Magnetic energy spectrum at the saturated stage of fluctuating MHD dynamo for the Mach number $M \approx 0.11$ (numerical simulation).

It is widely believed that the background emission's photons (cosmic microwave background – CMB) were mainly produced at the lepto/baryogenesis epoch and later were set free at the recombination (last scattering) epoch. Since the lepto/baryogenesis, magnetogenesis, the parity violation dominated by the magnetic helicity and the emission of the CMB-to-be photons are strongly interrelated one can expect that the level of the randomness of the magnetic field generated at the lepto/baryogenesis epoch will be imprinted on the level of randomness of the temperature of the CMB-to-be photons.

The continuing inflation smoothed out the strong fluctuations characterizing the lepto/baryogenesis epoch. At the recombination epoch, only tiny remnants of these fluctuations were present in the matter's motion and CMB. The remnants of the randomness, peculiar to the lepto/baryogenesis epoch's fluctuations, could also be preserved in the spatial power spectrum of the CMB temperature fluctuations (anisotropies) after the last scattering. Of course, this spectrum is a superposition of the remnant of the turbulent lepto/baryogenesis epoch, acoustic oscillations, etc. However, one can hope this remnant can be seen in the observed CMB spectrum and provide some information about the physical process at the lepto/baryogenesis epoch (see also an interesting discussion of present attempts to approach the problem in a recent paper[14] and references therein).

The observational estimates of the magnetic fields of the galaxy clusters turned out to be much larger than those predicted for the primordial magnetic fields. Therefore, different mechanisms of amplification of the seed magnetic fields (which supposedly came from the primordial stage) by the intensive (chaotic/turbulent) motion of the electrically conducting galaxy cluster plasmas were suggested in the literature. In the galaxy clusters, the chaotic/turbulent motion could be generated by cluster mergers, structure formation shocks, active galactic nuclei outflows, and the moving galaxy wakes.

Numerous models (numerical simulations) of the galaxy clusters magnetohydrodynamic dynamo were suggested (see, for instance[15][16][17] and references therein). Some recent models will be discussed below in detail.

There are certain hints of a parity violation in the magnetized intracluster plasmas. However, it is not clear whether the magnetic helicity in this case has a primordial origin or generated by the turbulent motion of the intracluster plasmas. Till now, technically, all observables related to the galaxy clusters' magnetic fields are entangled and mixed with other physical characteristics of the magnetized plasmas (electron density, for instance). The observable Faraday rotation maps were used to infer information about the intracluster magnetic field (see, for instance[18]). It will be shown below that the chaotic/turbulent magnetic field with the parity violation imprints its level of randomness on the Faraday rotation measure (cf the situation with the CMB above).

II. Deterministic chaos in magnetized plasma

In a recent paper[19] a numerical simulation of a small-scale (fluctuating) dynamo with parameters favorable to deterministic chaos was performed using magnetohydrodynamic (MHD) equations

$$\frac{\partial \rho}{\partial t}+\nabla \cdot (\rho \mathbf{u}) = 0, \tag{3}$$

$$\frac{\partial \mathbf{b}}{\partial t}= \nabla \times (\mathbf{u} \times \mathbf{b}) + \eta \nabla^2 \mathbf{b}, \tag{4}$$

$$\frac{\partial \mathbf{u}}{\partial t}+(\mathbf{u} \cdot \nabla) \mathbf{u} = -\frac{\nabla p}{\rho} + \frac{\mathbf{j} \times \mathbf{b}}{c \rho}+\nu \left(\nabla^2 \mathbf{u} + \frac{1}{3} \nabla (\nabla \cdot \mathbf{u}) + 2 \mathbf{S} \cdot \nabla \ln \rho \right) + \mathbf{F}, \tag{5}$$

in a triply-periodic cubic domain. In these equations $\mathbf{u}$ is the plasma velocity field, $\mathbf{b}$ is the divergence-free magnetic field, ρ is the plasma density, p is the plasma pressure, ν is the plasma viscosity, η is the plasma magnetic diffusivity, $\mathbf{j} = (c/4\pi) \nabla \times \mathbf{b}$ was taken for electric current density, c is the speed of light, $S_{ij} = \frac{1}{2} \left(u_{i,j} + u_{j,i} - \frac{2}{3} \delta_{ij} \nabla \cdot \mathbf{u} \right)$ was taken for the rate-of-strain tensor, and $\mathbf{F}$ is a random delta-

correlated in time solenoidal forcing function. An isothermal equation of state, $p = c_s^2 \rho$, was assumed with constant sound speed c_s.

The Reynolds and magnetic Reynolds numbers $Re = Re_m = 1122$, the Mach number $M \approx 0.11$, and the magnetic Prandtl number $Pr_m = 1$. A weak random magnetic field (with zero net flux across the computational domain) was used as an initial seed field.

Fig. 1 shows the one-dimensional (shell-averaged) magnetic energy spectrum at the saturated stage of the dynamo (the spectral data were taken from Fig. 2 of the paper[19]). The dashed curve is the best fit corresponding to Eq. (2) (deterministic chaos).

III. Distributed chaos dominated by magnetic helicity

The ideal MHD has three fundamental quadratic invariants: total energy, cross and magnetic helicity[20]. The validity of magnetic helicity conservation increases with the magnetic Reynolds number value Re_m.

The average magnetic helicity density is

$$h_m = \langle \mathbf{a}\mathbf{b} \rangle \tag{6}$$

here $\mathbf{a}$ is the vector potential, $\mathbf{b} = [\nabla \times \mathbf{a}]$ is the fluctuating magnetic field, and $\langle \ldots \rangle$ means spatial average (for the fluctuating variables $\langle \mathbf{a} \rangle = \langle \mathbf{b} \rangle = 0$).

The magnetic helicity can be considered as an adiabatic invariant not only in the ideal MHD but also in a weakly dissipative magnetized plasma (see for instance[21]), that makes it especially interesting for real astrophysical plasmas.

The transition from deterministic chaos to distributed one can be considered as a randomization. Namely, the change of physical parameters can result in the random fluctuations of the characteristic scale k_c in equation (2). One has to take this phenomenon into account. It can be done using an ensemble averaging

$$E(k) \propto \int_0^\infty P(k_c) \exp -(k/k_c) dk_c \tag{7}$$

Here a probability distribution $P(k_c)$ describes the random fluctuations of k_c. This is the rationale behind the name ‘distributed chaos’.

For the magnetic field dynamics dominated by the magnetic helicity the scaling relationship between characteristic values of k_c and B_c based on dimensional considerations

$$B_c \propto |h_m|^{1/2} k_c^{1/2} \tag{8}$$

can be used to find the probability distribution $P(k_c)$.

The value of B_c can be taken half-normally distributed $P(B_c) \propto \exp -(B_c^2/2\sigma^2)$[22]. It is a normal distribution with zero mean which is truncated to have a nonzero probability density function for positive values of its argument only. For instance, if B is a normally distributed random variable, then the variable $B_c = |B|$ is half-normally distributed[23].

From Eq. (8) we then obtain

$$P(k_c) \propto k_c^{-1/2} \exp -(k_c/4k_\beta) \tag{9}$$

It is the chi-squared probability distribution where k_β is a new constant).

Substituting Eq. (9) into Eq. (7) one obtains

$$E(k) \propto \exp -(k/k_\beta)^{1/2} \tag{10}$$

IV. Spontaneous breaking of local reflection symmetry

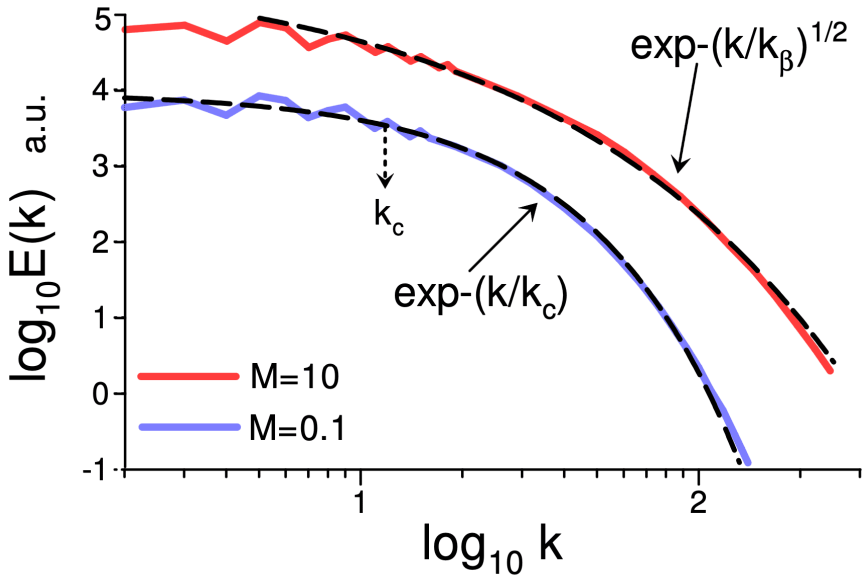

Figure 2. Magnetic energy spectra at the saturated stage of the fluctuating MHD dynamo for the Mach numbers $M = 0.1$ (bottom) and $M = 10$ (top). Numerical simulations.

For chaotic/turbulent flows with global reflection symmetry the net magnetic helicity is equal to zero, whereas the point-wise magnetic helicity is not (because of the spontaneous breaking of the local reflection symmetry, see Introduction). The spontaneous local symmetry breaking in such flows is accompanied by the emergence of the blobs with non-zero magnetic helicity[20][7][24][6]. The magnetic surfaces of these blobs can be defined by the boundary conditions: $\mathbf{b_n} \cdot \mathbf{n} = 0$, where $\mathbf{n}$ is a unit vector normal to the boundary of the blob. The magnetic helicity (and its adiabatic conservation) suppresses energy dissipation in such blobs considerably[24], that results in the long-term survival of these blobs in chaotic/turbulent environments.

The sign-defined magnetic helicity of the j-blob can be defined as

$$H_j^{\pm} = \int_{V_j} (\mathbf{a}(\mathbf{x},t) \cdot \mathbf{b}(\mathbf{x},t)) d\mathbf{x} \tag{11}$$

where ('+' or '-') denotes the blob's helicity sign. The $H_j^{\pm}$ is an adiabatic invariant[20].

Then we can consider the total sign-defined adiabatic invariant

$$I^{\pm} = \lim_{V \to \infty} \frac{1}{V} \sum_j H_j^{\pm} \tag{12}$$

The summation takes into account the blobs with a certain sign only ('+' or '–'), and V is the total volume of the blobs taken into account.

The adiabatic invariant $I^{\pm}$ defined by Eq. (12) can be used instead of the averaged magnetic helicity density h_m in the above estimate Eq. (8) for the special case of the local reflection symmetry breaking

$$B_c \propto |I^{\pm}|^{1/2} k_c^{1/2} \tag{13}$$

and the spectrum Eq. (10) can be also obtained for this case.

In recent papers[25][26] numerical simulations similar to that considered in Section II were performed (the net magnetic helicity was also negligible), but in these simulations the large Mach number $M = 10$ was achieved. Figure 2 shows the magnetic energy spectra computed in these numerical simulations. The spectral data shown in this figure were taken from Fig. C4 of the Ref.[26]. While for the small Mach number $M = 0.1$ the bottom dashed curve in Fig. 2 indicates the exponential spectrum Eq. (2) (deterministic chaos, cf Fig. 1), for the large Mach number $M = 10$ the top dashed curve indicates a stretched exponential spectrum Eq. (10) with $\beta = 1/2$. This indicates the distributed chaos dominated by magnetic helicity, i.e. the spontaneous breaking of local reflection symmetry.

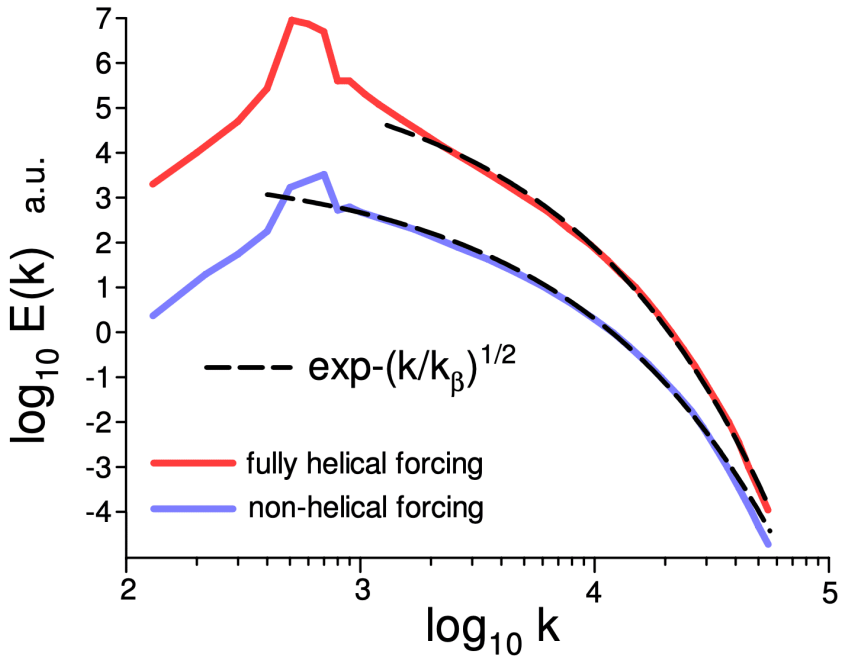

Figure 3. Magnetic energy spectra in an expanding flat universe at the radiation-dominated epoch after the electro-weak phase transition (numerical simulations). The spectra are vertically shifted for clarity.

doi.org/10.32388/PZ51AR

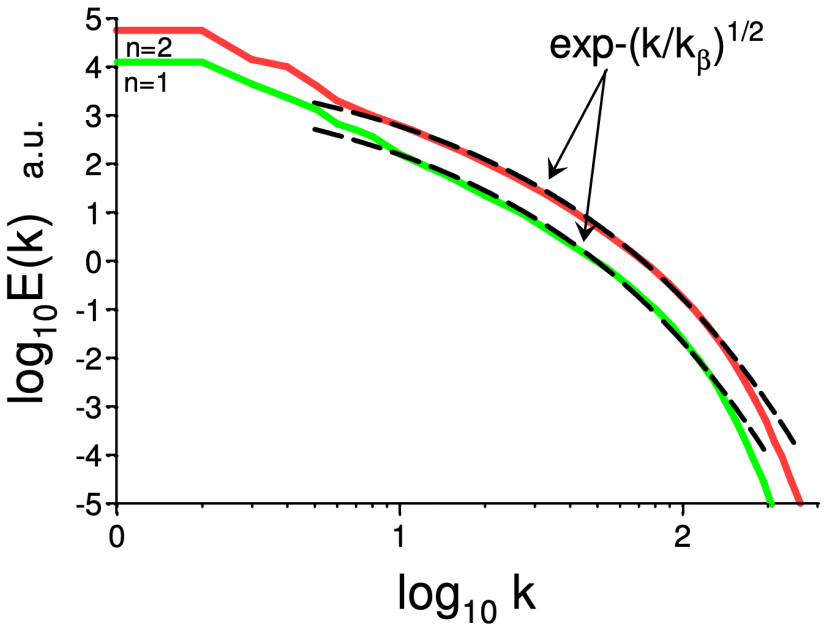

Figure 4. Magnetic energy spectra in relativistic fermion's plasmas generated due to a nonzero chiral chemical potential fluctuations μ_5 (numerical simulations). The spectra are vertically shifted for clarity.

In a recent paper[27] numerical simulations of magnetized ultrarelativistic plasma in an expanding flat universe at the radiation-dominated epoch after the electro-weak phase transition were performed using the comoving equations

$$\frac{\partial \ln \rho}{\partial t} = -\frac{4}{3}(\nabla \cdot \mathbf{u} + \mathbf{u} \cdot \nabla \ln\rho) + \frac{1}{\rho}\left[\mathbf{u} \cdot (\mathbf{J} \times \mathbf{B}) + \eta \mathbf{J}^2\right], \tag{14}$$

$$\frac{\partial \mathbf{u}}{\partial t} = -\mathbf{u} \cdot \nabla \mathbf{u} + \frac{\mathbf{u}}{3}(\nabla \cdot \mathbf{u} + \mathbf{u} \cdot \nabla \ln\rho) + \frac{2}{\rho}\nabla \cdot (\rho \nu \mathbf{S}) - \frac{1}{4}\nabla \ln\rho - \frac{\mathbf{u}}{\rho}\left[\mathbf{u} \cdot (\mathbf{J} \times \mathbf{B}) + \eta \mathbf{J}^2\right] + \frac{3}{4\rho}\mathbf{J} \times \mathbf{B}, \tag{15}$$

$$\frac{\partial \mathbf{B}}{\partial t} = \nabla \times (\mathbf{u} \times \mathbf{B} - \eta \mathbf{J} + \mathbf{F}). \tag{16}$$

The random electromotive force $\mathbf{F}$ simulates the generation of magnetic fields and was activated for a short duration (10% of the Hubble time). Two forcing cases were considered: fully helical and with negligible helicity. The simulations were performed in a periodic cubic box. The magnetic Pandtl number $Pr_m = \nu/\eta = 1$.

The magnetic energy spectra shown in Fig. 3 were computed at the time when the magnetic energy density reached its maximum. The spectral data were taken from Figs. 2 and 3 of the Ref.[27]. The dashed

curves indicate the magnetic helicity-dominated spectrum Eq. (10) for both cases: with fully helical (top) and non-helical (bottom) forcing. In the latter case, one can recognize the spontaneous parity violation caused by the chaotic/turbulent dynamics of the magnetized primordial plasma.

The above-discussed macroscopic mechanism of the chaotic/turbulent parity breaking and magnetic helicity generation can also boost the microscopic mechanisms of the parity breaking and magnetic helicity generation. Let us consider an example.

In a recent paper[28], the generation of the large-scale magnetic field in relativistic fermion's plasmas due to a nonzero chiral chemical potential fluctuations μ_5 (at initial $\langle \mu_5 \rangle = 0$) were studied using direct numerical simulation. The nonzero chiral potential appears in spatial areas of plasma where the chemical potentials of right and left-handed fermions are different. The chiral magnetohydrodynamic equations were used for this purpose

$$\frac{\partial \mathbf{B}}{\partial t} = \nabla \times [\mathbf{u} \times \mathbf{B} - \eta (\nabla \times \mathbf{B} - \mu_5 \mathbf{B})], \tag{17}$$

$$\rho \frac{D \mathbf{u}}{D t} = (\nabla \times \mathbf{B}) \times \mathbf{B} - \nabla p + \nabla \cdot (2 \nu \rho \mathbf{S}), \tag{18}$$

$$\frac{D \rho}{D t} = -\rho \nabla \cdot \mathbf{u}, \tag{19}$$

$$\frac{D \mu_5}{D t} = \mathcal{D}_5(\mu_5) + \lambda \eta \left[\mathbf{B} \cdot (\nabla \times \mathbf{B}) - \mu_5 \mathbf{B}^2 \right], \tag{20}$$

where λ is the chiral feedback parameter, the hyperdiffusion operator $\mathcal{D}_5(\mu_5) = -\mathcal{D}_5 \nabla^4 \mu_5$. Unlike the standard MHD, here one can speak about the conservation of total chirality $\langle \mathbf{A} \cdot \mathbf{B} \rangle + 2 \langle \mu_5 \rangle / \lambda$ (for $\langle \mu_5 \rangle = 0$ it is the magnetic helicity). The isothermal equation of state $p = \rho c_s^2$ relates pressure and density.

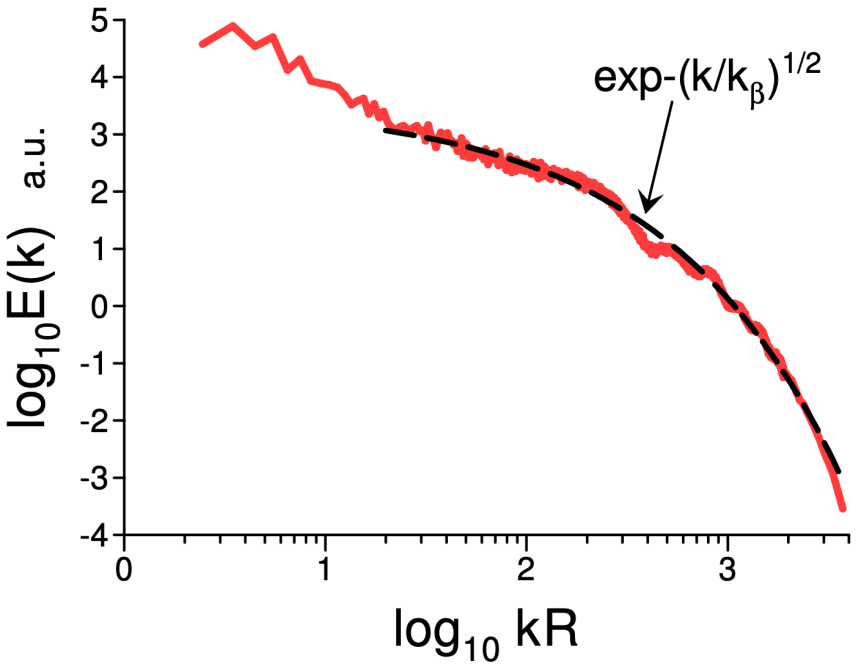

Figure 5. Power spectrum of CMB temperature fluctuations: Planck + ACT.

The equations were numerically solved in a periodic spatial box. Initial fluctuations of the chiral chemical potential μ_5 were taken as a Gaussian noise with spectrum $E_5(t_0) \propto k^{-n} \exp\left(-k^2/k_{cut}^2\right)$. The initial $\langle \mu_5 \rangle = 0$, and the initial magnetic helicity was negligible. The initial velocity field was absent, whereas initial (seed) magnetic field fluctuations were small. The dynamo was activated on small spatial scales due to the initial fluctuations of the chiral chemical potential, the Lorentz forces generated the magnetically dominated chaotic/turbulent plasma motion, and the inverse cascade (related to the magnetic helicity conservation) supposedly produced the large-scale magnetic field.

We will consider the runs performed with $n = 1, 2$. Figure 4 shows the magnetic energy spectra computed when the peak of the dynamo magnetic energy had the size of the computational box. The spectral data for Fig. 4 were taken from Fig. 4 of the Ref.[28].

The dashed curves indicate correspondence to the stretched exponential Eq. (10).

doi.org/10.32388/PZ51AR

V. Signature of the parity violation at the lepto-baryogenesis epoch in the CMB spectrum

Figure 5 shows a combined (Planck+ACT) power spectrum of CMB temperature fluctuations obtained by the Planck mission and Atacama cosmology telescope (ACT). The CMB data shown in Fig. 5 were cleaned from the foreground by the Planck and ATC teams. The spectral data were taken from the corresponding sites[29][30]. The ACT data were used for $kR > 1900$.

At the Planck and ACT sites the spectral data are given for the angular power spectra C_l vs the spherical multipole (or spherical harmonic degree) l. Using a 2D plane wavevector approximation[31] the spherical multipole l can be related to a wavenumber $k_l = \sqrt{l(l+1)}/R$, where R is the sphere's radius, and the azimuthally averaged 2D power spectral density $E(k_l) \approx R^2 C_l/\pi$[31].

The dashed curve indicates correspondence to the stretched exponential spectrum Eq. (10). With the assumption that the magnetic field at the lepto/baryogenesis epoch imprints its level of randomization on the temperature of the CMB–to–be photons (see Introduction), Fig. 5 can be considered as an indication that the remnant spectrum from the lepto/baryogenesis epoch can indeed be seen in the CMB spectrum. The waviness of the spectrum can be related to the acoustic oscillations. The randomization with $\beta = 1/2$ provides evidence of the parity violation and the magnetic helicity domination over the emission of the CMB-to-be photons at this epoch (at least for the middle and small scales).

VI. Magnetic field in galaxy clusters and Faraday rotation maps

A. Numerical simulations

The numerical models (simulations) not only allow a better understanding of the relevant physical processes but they become indispensable because of a principal difficulty of measurements (observations) of galaxy clusters' magnetic fields. Till now technically all observables related to the galaxy clusters' magnetic fields are entangled and mixed with other physical characteristics of the magnetized plasmas (electron density, for instance).

In a paper[32] spectra of the magnetic energy and corresponding spectra of the Faraday rotational measure maps were computed in the framework of the standard (collisional) magnetohydrodynamics

and in the framework of a collisionless MHD model (which is expected to be more appropriate to the magnetized and weakly collisional intracluster plasma). This model is based on the dynamic equations

$$\frac{\partial \rho}{\partial t} + \nabla \cdot (\rho \mathbf{u}) = 0, \tag{21}$$

$$\frac{\partial (\rho \mathbf{u})}{\partial t} + \nabla \cdot \left[\rho \mathbf{u}\mathbf{u} + \left(\mathbf{P} + \frac{B^2}{8\pi} \right) \mathbf{I} - \frac{\mathbf{B}\mathbf{B}}{4\pi} \right] = \mathbf{f}, \tag{22}$$

$$\frac{\partial \mathbf{B}}{\partial t} - \nabla \times (\mathbf{u} \times \mathbf{B}) = 0, \tag{23}$$

where the pressure tensor is

$$\mathbf{P} = p_\perp \mathbf{I} + (p_\parallel - p_\perp) \hat{b}\hat{b}, \tag{24}$$

here $p_\perp = c_\perp^2 \rho$, $p_\parallel = c_\parallel^2 \rho$, $\hat{b} = \mathbf{B}/|\mathbf{B}|$, and $c_\perp$ and $c_\parallel$ are the sound speeds perpendicular and parallel to the magnetic field $\mathbf{B}$, correspondingly.

The authors of the paper[32] reported some indications of a small-scale (fluctuation) dynamo in work for their models.

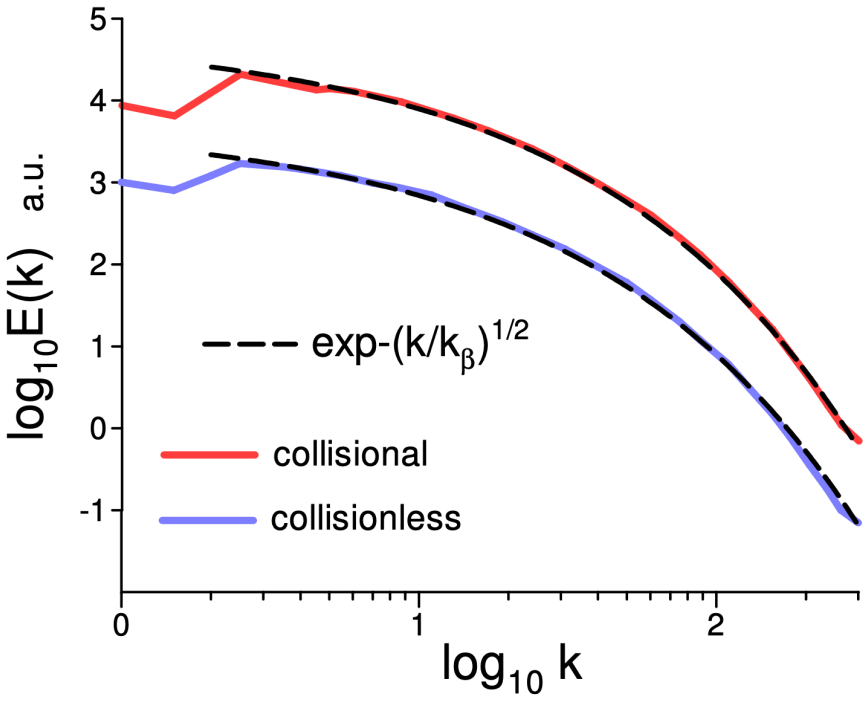

Figure 6. Magnetic energy spectra computed for the collisional (top) and collisionless (bottom) magnetohydrodynamics. The spectra are vertically shifted for clarity.

doi.org/10.32388/PZ51AR

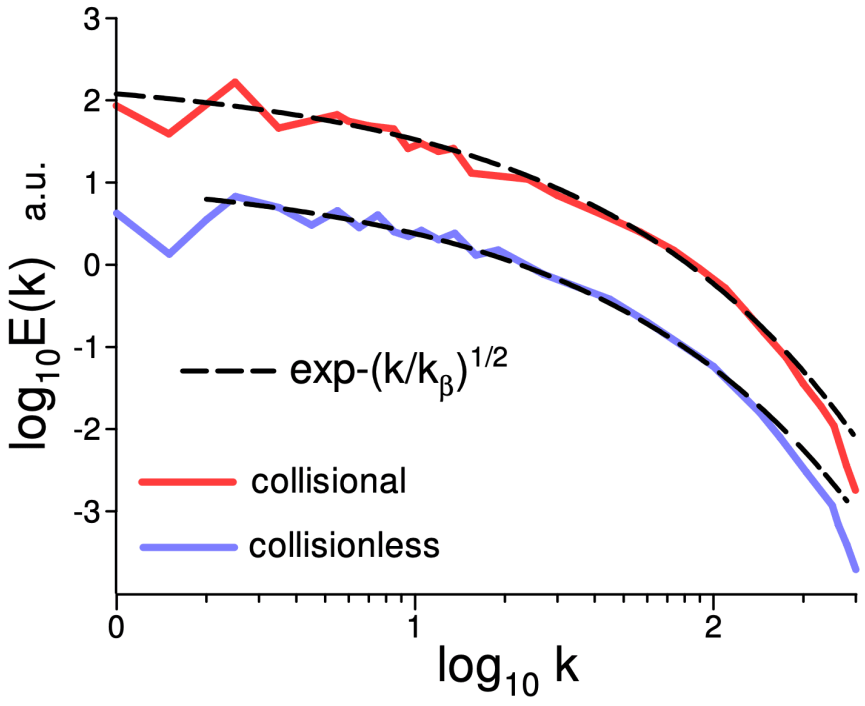

Figure 7. Power spectra of the Faraday rotational measure maps computed for the collisional (top) and collisionless (bottom) magnetohydrodynamics. The spectra are vertically shifted for clarity.

doi.org/10.32388/PZ51AR

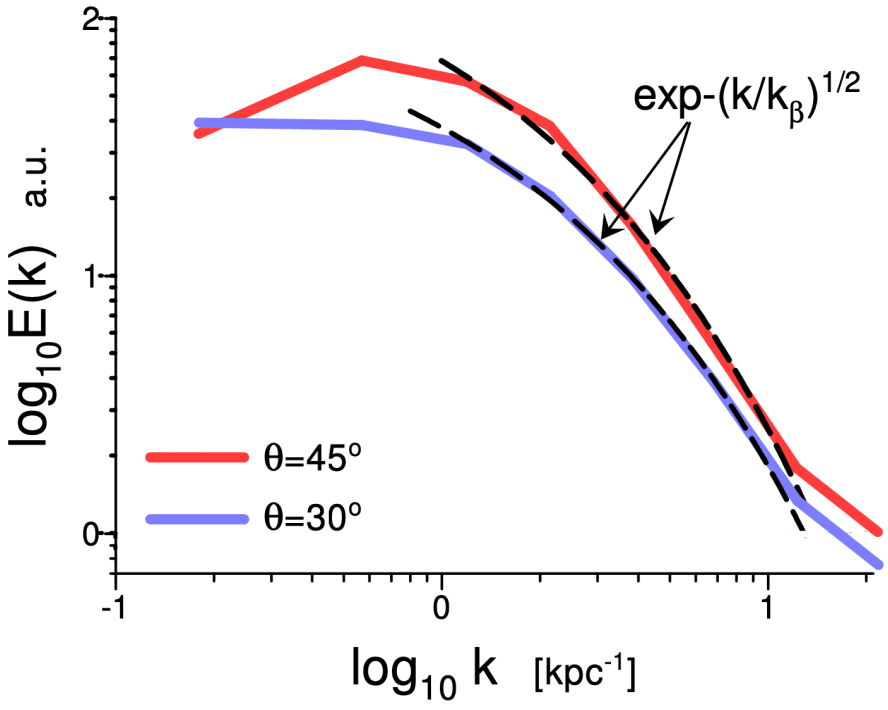

Figure 8. Intracluster magnetic power spectra for the northern radio lobe of Hydra A for two values of the inclination angles (between the line of sight and the northern lobe) $\theta = 45^o$ (top) and $\theta = 30^o$ (bottom).

doi.org/10.32388/PZ51AR

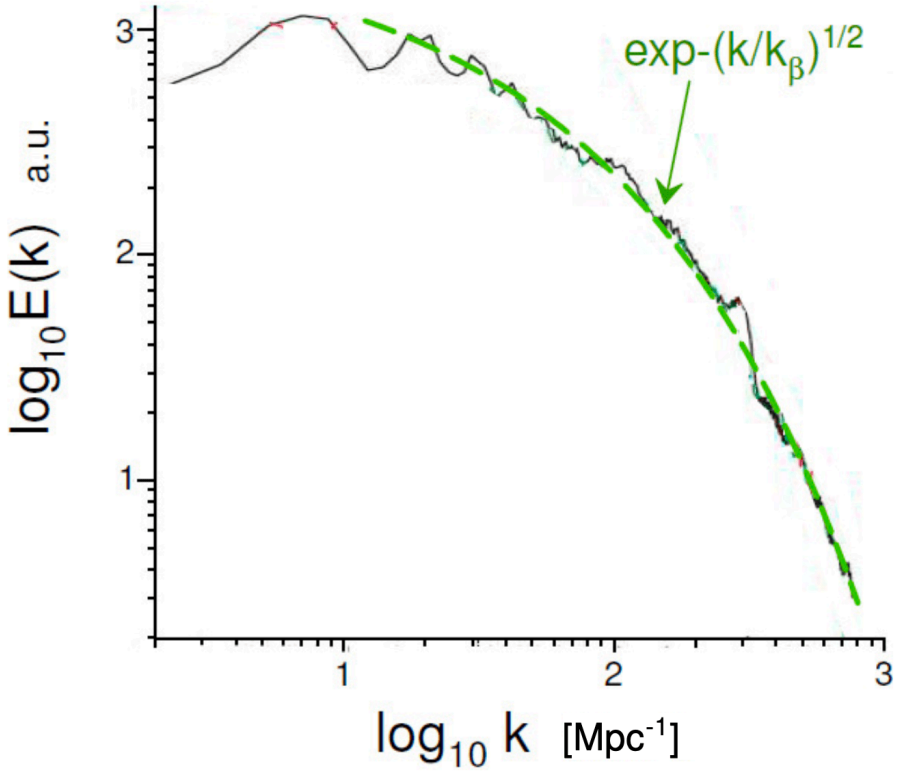

Figure 9. Radially averaged power spectrum of a Faraday rotation measure map for the galaxy cluster A119 .

Figure 6 shows the spectra of magnetic energy computed for the collisional (top) and collisionless (bottom) magnetohydrodynamics with a weak uniform external magnetic field $B_{ext} = 0.1$ and sound speed $c_{snd} = 0.1$ for collisional and $c_{||} = 0.1$, $c_{\perp} = 0.05$ for collisionless cases (in terms of Ref.[32]). The spectral data were taken from Figs. 6a and 6b of the paper[32]. The dashed curves indicate the best fit by the stretched exponential Eq. (10).

One can see that for both models interpretation of the spectral data for magnetic energy using the notion of the distributed chaos dominated by magnetic helicity Eq. (10) is in good agreement with the results of the numerical simulations.

Figure 7 shows the power spectra of the Faraday rotational measure maps corresponding to Fig. 6. The spectral data were taken from Figs 12a,c of the paper[32]. The dashed curves indicate the best fit by the stretched exponential Eq. (10).

One can see that the magnetic field imprints its level of randomization on the Faraday maps. Therefore, the observational Faraday rotation measure maps could be used to obtain this information about the magnetic fields.

B. Observations

In a paper[18], the Faraday rotation maps of the northern radio lobe of Hydra A (a cool core galaxy cluster) were analyzed with a Bayesian maximum likelihood analysis to infer the intracluster magnetic field power spectrum. Figure 8 shows the magnetic power spectra for two values of the inclination angles (between the line of sight and the northern lobe) $\theta = 45^o$ (top) and $\theta = 30^o$ (bottom). The spectral data were taken from Fig. 7 of the paper[18].

The dashed curve indicates the best fit by the stretched exponential Eq. (10) (cf previous section).

Figure 9 shows the radially averaged power spectrum of a Faraday rotation measure map for the galaxy cluster A119 (the spectral data were taken from Fig. 10d of paper[33]. This galaxy cluster is located in a region with a rather low Galactic rotation measure and consists of three extended radio galaxies. These galaxies are located at different projected distances (170, 453, and 1515 kpc) from the cluster center and the radio sources are highly polarized.

The dashed curve indicates the best fit by the stretched exponential Eq. (10).

Acknowledgements

I thank E. Levich, H.K. Moffatt, S. Pikovsky, and K.R. Sreenivasan for stimulating discussions. I also thank the Planck and ACT teams for sharing their data.

References

1. ^*Subramanian K. The origin, evolution and signatures of primordial magnetic fields. Rep. Prog. Phys. 79, 07 690 (2016).*
2. ^*Kamada K. Return of grand unified theory baryogenesis: Source of helical hypermagnetic fields for the ba ryon asymmetry of the universe. Phys. Rev. D 97, 103506 (2018).*
3. ^*R.M. Kerr, Helicity generation in 3D Euler and turbulence, in: Elementary Vortices and Coherent Structures, Proceedings of the IUTAM Symposium Kyoto, 2004, 1–8.*

4. ^Holm D.D, Kerr R.M. Transient vortex events in the initial value problem for turbulence. Phys. Rev. Lett. 88, 244501 (2002).
5. ^Holm D.D, Kerr R.M. Helicity in the formation of turbulence. Physics of Fluids 19, 025101 (2007).
6. a, b, cMoffatt H.K. Magnetostatic equilibria and analogous Euler flows of arbitrarily complex topology. Part 1. Fundamentals. J. Fluid Mech. 159, 359–378 (1985).
7. a, b, cBershadskii A. Magneto-inertial range dominated by magnetic helicity in space plasmas. Fundamenta l Plasma Physics 11, 100066 (2024).
8. ^Semikoz V.B, Sokoloff D.D. Effects of P-Noninvariance, Particles, and Dynamos, in: Helicities in Geophysics, Astrophysics and Beyond (Eds. K. Kuzanyan, N. Yokoi, M.K. Georgoulis, R. Stepanov) AGU, 2023.
9. ^Maggs J.E, Morales G.J. Generality of deterministic chaos, exponential spectra, and Lorentzian pulses in ma gnetically confined plasmas. Phys. Rev. Lett. 107, 85003 (2011).
10. ^Maggs J.E, Morales G.J. Origin of Lorentzian pulses in deterministic chaos. Phys. Rev. E 86, 015401(R) (201 2).
11. ^Maggs J.E, Morales G.J. Exponential power spectra, deterministic chaos and Lorentzian pulses in plasma e dge dynamics. Plasma Phys. Control. Fusion 54, 124041 (2012).
12. ^Khurshid S, Donzis D.A, Sreenivasan K.R. Energy spectrum in the dissipation range. Phys. Rev. Fluids 3, 082 601(R) (2018).
13. a, bWu Z.-Z, Kadanoff L.P, Libchaber A, Sano M. Frequency power spectrum of temperature fluctuations in fr ee convection. Phys. Rev. Lett. 64, 2140-2143 (1990).
14. ^Philcox O.H.E. Do the CMB Temperature Fluctuations Conserve Parity? Phys. Rev. Lett. 31, 181001 (2023).
15. ^Ruzmaikin A, Sokoloff D, Shukurov A. The dynamo origin of magnetic fields in galaxy clusters. MNRAS 24 1, 1-14 (1989).
16. ^Vazza F, Brüggen M, Gheller C, Wang P. On the amplification of magnetic fields in cosmic filaments and ga laxy clusters. MNRAS 445, 3706–3722 (2014).
17. ^Subramanian K. From primordial seed magnetic fields to the galactic dynamo. Galaxies 7, 47 (2019).
18. a, b, cVogt C, Enßlin T.A. A Bayesian view on Faraday rotation maps – Seeing the magnetic power spectra in galaxy clusters. A&A 434, 67-76 (2005).
19. a, bSeta A, Bushby P.J, Shukurov A, Wood T.S. Saturation mechanism of the fluctuation dynamo {Pr_{m}}≥1. Phys. Rev. Fluids 5, 043702 (2020).

20. a, b, c *Moffatt H.K, Tsinober A. Helicity in laminar and turbulent flow. Annu. Rev. Fluid Mech. 24, 281–312 (19 93).*

21. ^ *Zenati Y, Vishniac E.T. Conserving local magnetic helicity in numerical simulations. ApJ 948, 11 (2023).*

22. ^ *Monin A.S, Yaglom A.M. Statistical Fluid Mechanics, Vol. II: Mechanics of Turbulence, Dover Pub. NY, 2007.*

23. ^ *Johnson N.L, Kotz S, Balakrishnan N. Continuous Univariate Distributions, Vol. 1, Wiley NY, 1994.*

24. a, b *Moffatt H.K. The degree of knottedness of tangled vortex lines. J. Fluid Mech. 35, 117–129 (1969).*

25. ^ *Seta A, Federrath C. Magnetic fields in the Milky Way from pulsar observations: effect of the correlation be tween thermal electrons and magnetic fields. MNRAS 502, 2220–2237 (2021).*

26. a, b *Seta A, Federrath C, Livingston J.D, McClure-Griffiths N.M. Rotation measure structure functions with hig her-order stencils as a probe of small-scale magnetic fluctuations and its application to the Small and Larg e Magellanic Clouds. MNRAS 518, 919–944 (2023).*

27. a, b *Pol A.R, Mandal S, Brandenburg A, Kahniashvilif T. Polarization of gravitational waves from helical MH D turbulent sources. JCAP 04, 019 (2022).*

28. a, b *Schober J, Rogachevskii I, Brandenburg A. Production of a chiral magnetic anomaly with emerging turbu lence and mean-field dynamo action. Phys. Rev. Lett. 128, 065002 (2022).*

29. ^ *Available at the site https://pla.esac.esa.int/pla.*

30. ^ *Available at the site https://lambda.gsfc.nasa.gov/product/ act/.*

31. a, b *Maus S (2008). "The geomagnetic power spectrum". Geophys. J. Int.. 174: 135–142.*

32. a, b, c, d, e *Nakwacki MS, Kowal G, Santos-Lima R, de Gouveia Dal Pino EM, Falceta-Gonçalves DA (2016). "Fe atures of collisionless turbulence in the intracluster medium from simulated Faraday Rotation maps". MNR AS. 455: 3702–3723.*

33. ^ *Murgia M, Govoni F, Feretti L, Giovannini G, Dallacasa D, Fanti R, Taylor GB, Dolag K (2004). "Magnetic fiel ds and Faraday rotation in clusters of galaxies". A&A. 424: 429-446.*

Declarations

Funding: No specific funding was received for this work.

Potential competing interests: No potential competing interests to declare.